Hindawi Publishing Corporation
International Journal of Geophysics
Volume 2016, Article ID 7378920, 10 pages
http://dx.doi.org/10.1155/2016/7378920

Research Article

Study on Coulomb Stress Triggering of the April 2015 M7.8 Nepal Earthquake Sequence

Jianchao Wu,[1,2] Qing Hu,[1] Weijie Li,[2] and Dongning Lei[1]

[1]*Key Laboratory of Earthquake Geodesy, Institute of Seismology, CEA, Wuhan 430071, China*
[2]*Department of Mechanical Engineering, University of Houston, Houston, TX 77204, USA*

Correspondence should be addressed to Jianchao Wu; jianchaowu85@gmail.com

Received 26 July 2016; Revised 5 September 2016; Accepted 14 September 2016

Academic Editor: Bofeng Guo

In April 2015, a M7.8 earthquake occurred less than one month before a M7.3 earthquake near Kodari, Nepal. The Nepal earthquake sequences also include four larger (M > 6) aftershocks. To reveal the interrelation between the main shock and the aftershocks, we check the role of coseismic coulomb stress triggering on aftershocks that follow the M7.8 main shock. Based on the focal mechanisms of the aftershocks and source models of the main shock, the coulomb failure stress changes on both of the focal mechanism nodal planes are calculated. In addition, the coulomb stress changes on the focal sources of each aftershock are also calculated. A large proportion of the M > 6 aftershocks occurred in positive coulomb stress areas triggered by the M7.8 main shock. The secondary triggering effect of the M7.3 aftershock is also found in this paper. More specifically, the M7.3 aftershock promoted failure on the rupture plane of the M6.3 aftershock. Therefore, we may conclude that the majority of larger aftershocks, which accumulated positive coulomb stress changes during the sequence, were promoted or triggered by the main shock failure. It suggests that coulomb stress triggering contributed to the evolution of the Nepal M7.8 earthquake sequence.

1. Introduction

The 2015 Nepal M7.8 earthquake occurred as a result of thrust faulting near the main frontal thrust interface system between the subducting India plate and the overriding Eurasia plate to the north. The epicenter, size, and focal mechanism of the M7.8 earthquake are consistent with its occurrence on the detachment associated with the Main Himalayan Thrust, which defines the subduction thrust interface between the India and Eurasia plates (Figure 1). This event was followed by many aftershocks, the largest being an M7.3 earthquake on May 12, 17 days after the main shock. The M7.3 aftershock was located 150 km to the east, which ruptured much of the detachment between these two strong earthquakes. Among the aftershocks, there are four larger (M > 6) earthquakes.

After the great earthquake, there is often accompanied with a large number of aftershocks. What is the interrelation and interaction between the main shock and aftershocks? Aftershock activities may be promoted or triggered when the coulomb stress on the fault plane is increased by as little as 0.1 bar [1]. A small increase in coulomb failure stress due to the earlier shock activity can trigger subsequent aftershocks [2]. For the coulomb stress triggering, the elastic displacement model was established in 1990s [3]. Based on the elastic displacement model of great earthquakes, the coulomb failure stress changes on the receiver fault planes can be calculated and investigated. Researches on coulomb stress triggering in recent years show that the main earthquake could change the coulomb stress on the nearby faults plane and then make the aftershocks easy to occur or delayed to occur [4]. Here we investigate whether the calculating coulomb stress change from the main shock may have caused the cascading failure that triggers the subsequent aftershock sequence.

Previous studies of many earthquake cases show that the increased area of coulomb failure stress is obviously conducive to the subsequent aftershock occurrence but the decreased area is not conversely [5]. Based on the source models of the Nepal M7.8 earthquake, the static coulomb failure stress changes induced by the M7.8 main shock are calculated. Then we discuss the relationship between the coseismic coulomb stress changes and the aftershocks.

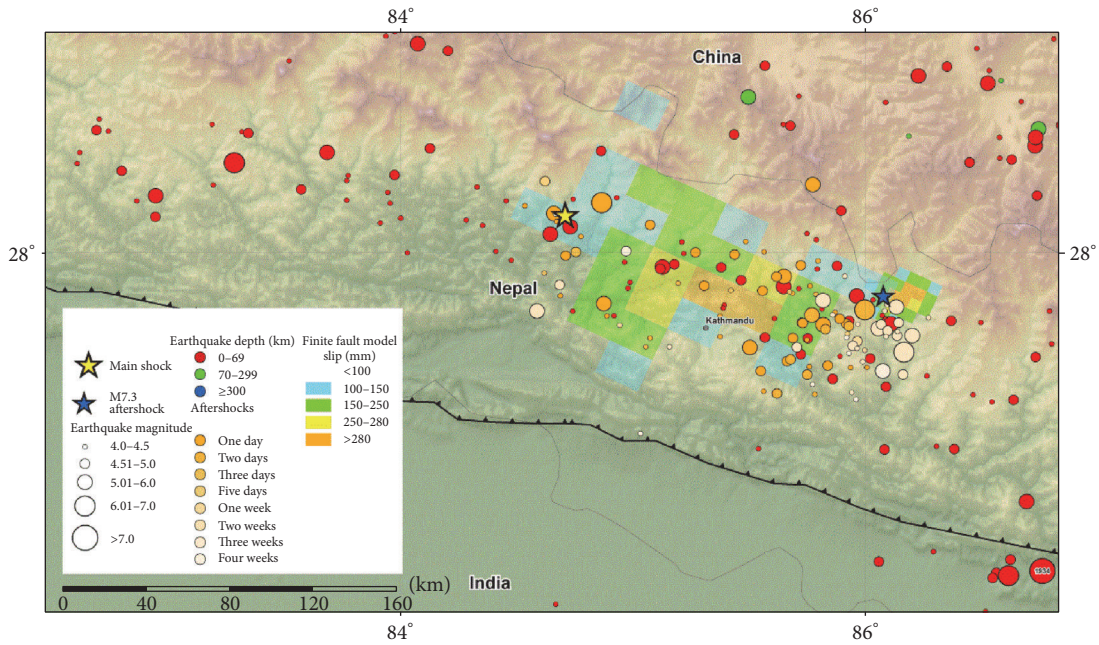

Figure 1: The epicentral region of the 2015 Nepal M7.8 earthquake sequence. At the location of this earthquake, the India plate is converging with Eurasia at a rate of 45 mm/yr towards the north-northeast, driving the uplift of the Himalayan mountain range (modified from USGS [6]).

In this paper, by using the Coulomb 3.3 program [4], which implements the elastic half space of Okada [3], we calculate the coulomb stress changes due to the main shock and investigate whether the M7.8 earthquake is responsible for the subsequent aftershock events. We also calculate the coulomb stress changes on the hypocenter of each aftershock. These analysis provide insight into whether the M7.8 earthquake results in a coulomb stress change that promotes failure of the subsequent aftershock sequence along the main thrust interface system.

2. Coulomb Stress Triggering Principle

The brittle failure of rock is due to the combination of normal and shear stress conditions according to the Coulomb-Mohr failure criterion [9]. The coulomb stress changes caused by the earlier earthquake can explain the epicenter location of aftershocks [10, 11]. The aftershocks probably occur in that location where the coulomb stress exceeds the failure strength of the fault surface. We can assume that the fault plane is developed in the rock and the internal friction coefficient will not change with time. Then, the fault plane will generate shear failure when the shear stress (τ) reaches the frictional strength (τ_f). Harris [12] defined ($\tau - \tau_f$) as Coulomb failure stress (CFS):

$$\mathrm{CFS} = \tau - \tau_f = \tau - s - \mu(\sigma_n - p), \quad (1)$$

where s is cohesion and μ is internal friction coefficient, respectively. σ_n is normal stress on the fault plane and p is pore pressure, respectively [5]. Then the change of coulomb failure stress is defined as follows:

$$\Delta\mathrm{CFS} = \Delta\tau + \mu(\Delta\sigma_n - \Delta p), \quad (2)$$

where $\Delta\tau$ is the shear stress in the direction of slip on the receiver fault plane. $\Delta\sigma_n$ is the normal stress change (positive for extension). Δp is the pore pressure change, and μ is the coefficient of friction, which ranges from 0.6 to 0.8 for most intact rocks [12]. Assuming the medium is homogeneous and isotropic, and the pore pressure change is related to the normal stress, so the above formula can be transformed into [5]

$$\Delta\mathrm{CFS} = \Delta\tau + \mu'\Delta\sigma, \quad (3)$$

where $\mu' = \mu(1 - \beta)$ is the apparent coefficient of friction. β is the Skempton's coefficient, which describes the change in pore pressure that results from a change in an externally applied stress and often ranges in value from 0.5 to 1.0 [13, 14]. The theoretical range of the apparent coefficient of friction is from 0 to 0.8 but is typically found to be around 0.4 [12, 15]. This value is commonly used in calculations of coulomb stress changes to minimize uncertainty [16]. Previous researchers adopted deduced values of $0.2 \le \mu' \le 0.75$ to calculate the coulomb failure stress changes, such as the 1979 Homestead Valley [17], 1984 Morgan Hill [18], 1987 Superstition Hills [19], and 1989 Loma Prieta earthquakes [10]. In this study, we examined $\mu' = 0.2$, 0.4, 0.6, and 0.8, respectively. We found that the coulomb failure changes only in detail with three different values, which is consistent with previous conclusions. So we take the calculation results with $\mu' = 0.4$ for the following analysis and discussion.

The strong earthquake could reduce the accumulated tectonic stress on the whole but result in partial stress increases that will trigger subsequent earthquakes. Aftershock activities are promoted when a fault plane or specified nodal plane experiences a stress increase, especially the increased value

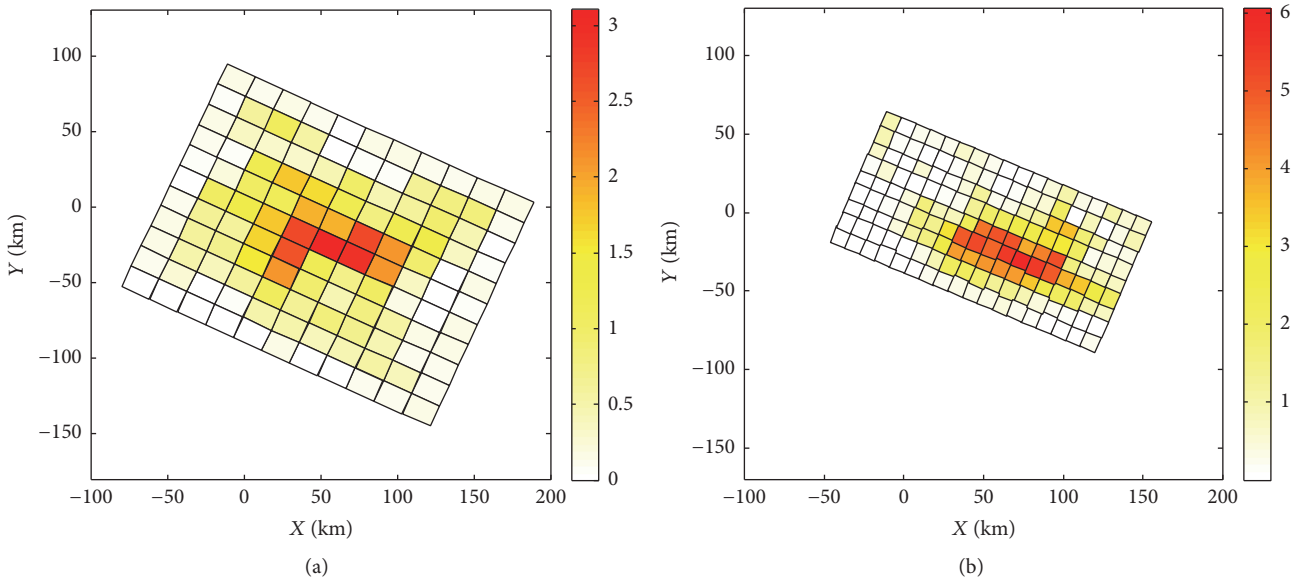

Figure 2: The source models of the Nepal M7.8 earthquake (unit: m). (a) is the finite fault model given by Gavin Hayes [7]; (b) is the kinematic rupture model inverted by Han Yue [8].

exceeds the assumed threshold value of 0.1 bar [1]. It means that the fault plane is near failure before the earthquake since the threshold is relatively low [20]. Based on the failure theory above, we study whether the aftershock activities occurred in regions of stress increase.The Dislocation Theory demonstrates the interrelation between the stress field on the discontinuous plane and surrounding around in the continuous medium. Based on the geometric parameters of earthquake dislocation plane, we can calculate the coulomb failure stress in the elastomer's interior [5]. In this study, we examine the coulomb failure stress changes caused by the M7.8 Nepal earthquake and reveal its triggering effect to the aftershocks with M > 6.

To calculate the reliable coulomb failure stress changes, we need to build a more realistic finite fault failure model. To compare the calculation results of the coulomb stress changes, we adopt two source models that had been inverted with different inversion techniques.

The first source model is inverted from Global Seismic Network (GSN) broadband waveforms by Gavin Hayes (Figure 2(a)) [7, 21]. Gavin Hayes had used GSN broadband waveforms downloaded from the National Earthquake Information Center (NEIC) waveform server and analyzed 42 teleseismic broadband P waveforms, 15 broadband SH waveforms, and 62 long period surface waves selected based on data quality and azimuthal distribution. Waveforms were first converted to displacement by removing the instrument response and then used to constrain the slip history using a finite fault inverse algorithm [22].

The second source model is given by Yue Han by exploring both a regularized multi-time-window approach and an unsmoothed Bayesian formulation (Figure 2(b)) [8, 23]. Yue Han had used a variety of datasets including teleseismic body wave records, static and high rate GPS observations, synthetic aperture radar (SAR) offset images, and interferometric SAR (InSAR). InSAR interferograms from ALOS-2, RADARSAT-2, and Sentinel-1a satellites were used in the joint inversion.

The two kinds of models are different in details, but they both show that the general azimuth of the fault plane is approximately consistent. Both of the results show that the Nepal M7.8 earthquake is characterized by unilateral rupture extending along strike direction approximately 70 km to the southeast and 40 km along dip direction. As shown in Figure 2, the different color indicates the amplitude of slip. The deeper the color, the greater the amount of the slip. For the M7.8 main shock, the strike of the fault rupture plane is 295° and the dip is 10° NNE. The rupture surface is approximately 220 km along strike and 180 km along downdip. The seismic moment release based upon this plane is $8.1e + 27$ dyne·cm.

3. Coulomb Stress Changes Derived on Assumed Rupture Planes

We collect the focal mechanisms of four M > 6 aftershocks from U.S. Geological Survey (USGS). Based on the source models of Gavin Hayes and Han Yue, with the Coulomb 3.3 program, we calculate the coulomb stress changes on both nodal planes of the high-quality focal mechanism solutions in their rake directions (Figures 3 and 4). The calculation of coulomb stress changes on the nodal planes of aftershock focal mechanism solutions is a direct application of the coulomb hypothesis.

The theory of stress triggering demonstrates that the receiving faults describe the comprehensive features of the areal faults. Different receiving faults reflect different responses of coulomb failure stress produced by the main shock. In this study, we use the nodal planes of the four M > 6 aftershocks from USGS and CMT. We consider both of the nodal plane of each aftershock as the receiving faults to make sure that there are no omissions. Thus, we calculate

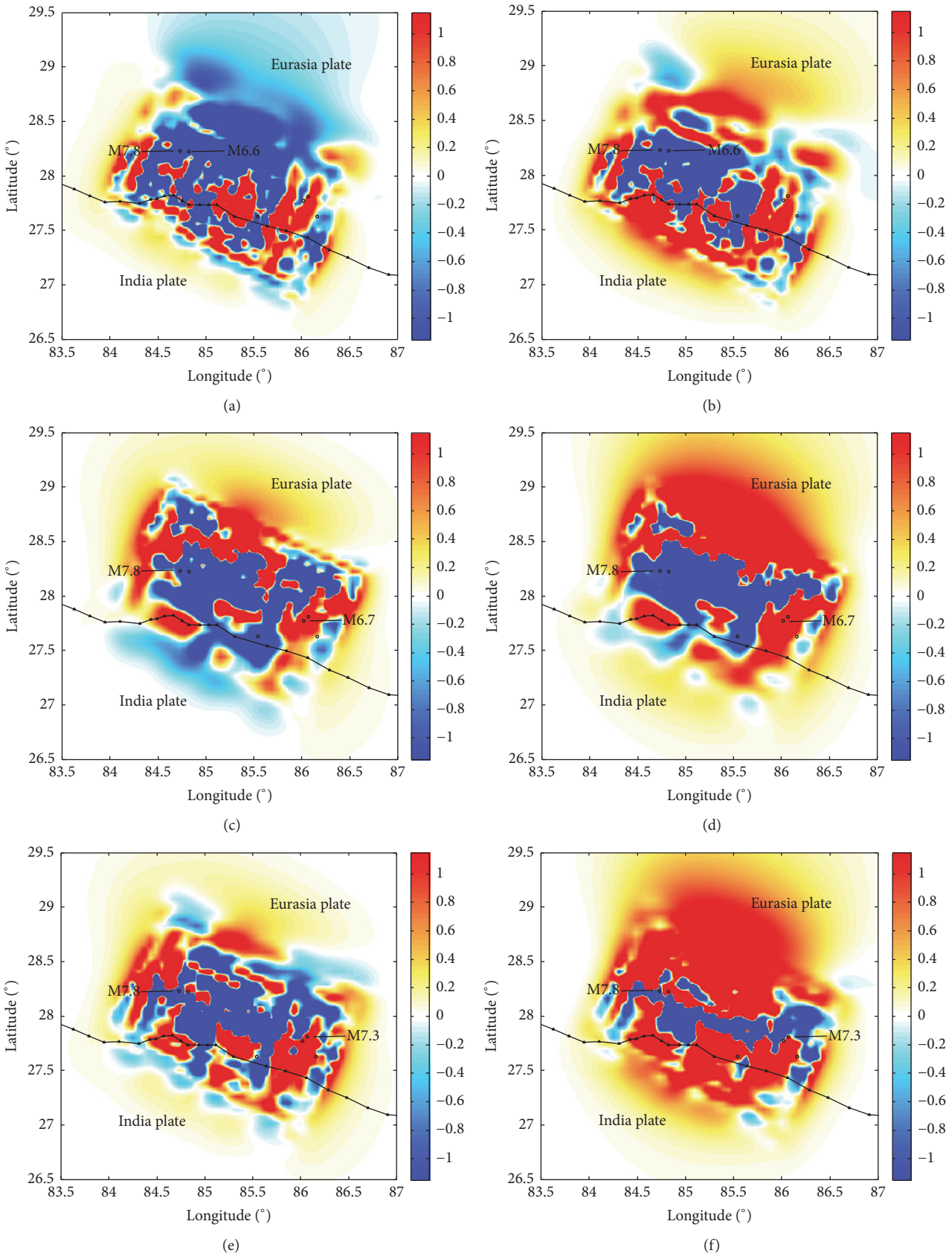

Figure 3: Continued.

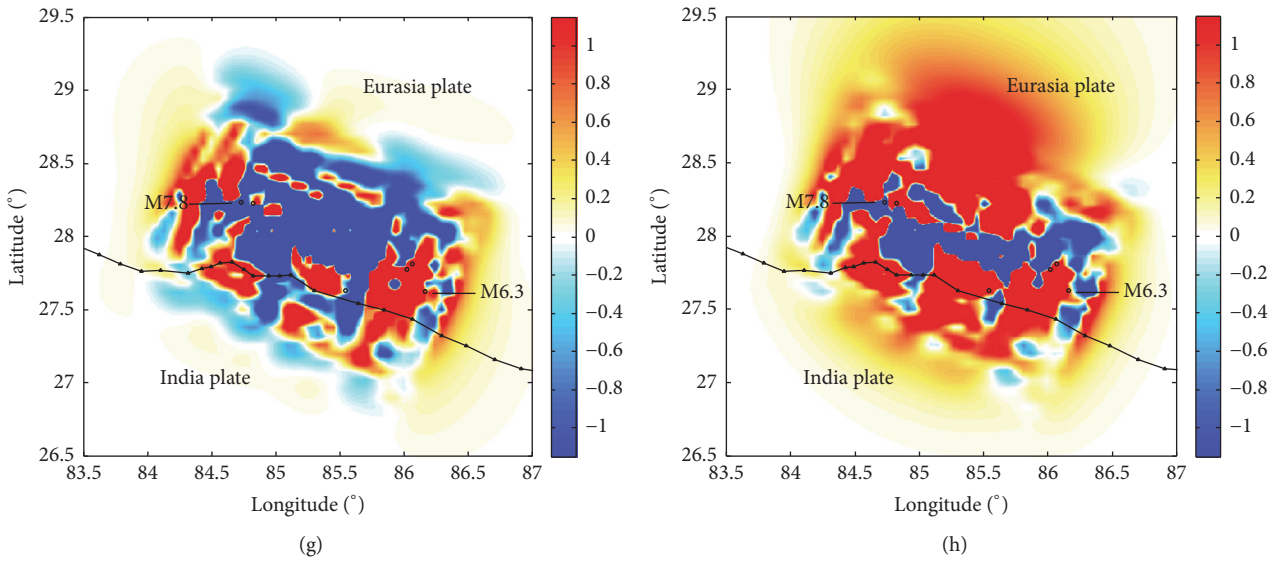

Figure 3: Coulomb stress changes on both nodal planes of 4 M > 6 aftershocks triggered by the 2015 Nepal M7.8 earthquake based on Gavin Hayes's finite fault model (unit: bar). (a) 2015-04-25, M6.6, nodal plane: 271, 21, 64, depth: 10.0 km; (b) 2015-04-25, M6.6, nodal plane: 119, 71, 100, depth: 10.0 km; (c) 2015-04-26, M6.7, nodal plane: 285, 12, 94, depth: 22.9 km; (d) 2015-04-26, M6.7, nodal plane: 100, 78, 89, depth: 22.9 km; (e) 2015-05-12, M7.3, nodal plane: 303, 9, 110, depth: 15.5 km; (f) 2015-05-12, M7.3, nodal plane: 102, 82, 87, depth: 15.5 km; (g) 2015-05-12, M6.3, nodal plane: 274, 14, 89, depth: 15.5 km; (h) 2015-05-12, M6.3, nodal plane: 95, 76, 90, depth: 15.5 km.

the coulomb stress change on the nodal plane that is most consistent with the orientation of rupture for the four larger aftershocks.

We assume that the model is a half-space elastic medium, and the Young's modulus is 8.0×10^5 bar. The Poisson's ratio is 0.25 and the effective friction coefficient is 0.4. The coulomb failure stress, produced by the Nepal M7.8 main shock on the rupture surface and focal depth of the aftershocks, is essential for us to explore the causes of the larger aftershocks.

Figure 3 shows the coulomb failure stress produced by the Nepal M7.8 earthquake on both nodal planes of the four M > 6 aftershocks based on Gavin Hayes's finite fault model. Figures 3 and 4 for each aftershock are different in detail due to representing two different nodal planes. Among the four M > 6 aftershocks, three of them occurred in the increased coulomb stress area. Conversely, the M7.8 exert a negative coulomb stress change on both of the nodal planes for the M6.6 aftershock. Overall, we observe that most of the aftershocks experience positive coulomb stress change that would promote or trigger failure.

Figure 4 demonstrates the coulomb failure stress caused by the Nepal M7.8 earthquake on both nodal planes of the four M > 6 aftershocks based on Yue Han's kinematic rupture model. As shown in Figure 4, the coulomb stress changes are quite different with Figure 3. However, there are at least two aspects in common. Firstly, there occurs a negative coulomb stress zone with a NW-SE direction near the M7.8 earthquake epicenter. In general, a large-magnitude earthquake decreases the stress along a fault. Secondly, three of the M > 6 aftershocks occurred in the positive coulomb stress area, which is consistent with the calculation results in Figure 3. In summary, we can conclude that most of the M > 6 aftershocks occurred in the area of increased coulomb stress. We can also make a further inference that most of the M > 6 aftershocks are triggered by the M7.8 earthquake.

It should be noted that both of the M7.3 and M6.3 aftershocks occurred on May 12, 2015. The M7.3 earthquake is 31 minutes earlier than the M6.3 event. The M6.3 aftershock epicenter lies 22 km to the south of the M7.3 earthquake. So, we were wondering if the M6.3 aftershock is promoted or triggered by the M7.3 earthquake. Based on the source modes of M7.3 earthquake inverted by Gavin Hayes and Han Yue, we also calculate the coulomb stress changes on both nodal planes of the M6.3 aftershock (Figures 5 and 6). We find that the coulomb stress change at the location of the M6.3 aftershock is consistent with triggering by the M7.3 earthquake. It means that both of the M7.8 and M7.3 earthquake promote or trigger the M6.3 aftershock.

4. Coulomb Stress Changes Estimated on the Focal Source

In this section, we also calculate the coulomb stress changes on the focal source inside the crust. The coulomb stress changes at the source point could be more accurate and appropriate to explain the stress triggering effect. Since the earthquake location accuracy is relatively low and the results of focal mechanism solutions given by different research institutes are different in details, we collect the USGS data to calculate the stress changes triggered by the M7.8 main shock (Table 1). Apart from this calculation, we also calculate the stress changes in the focal source of the M6.3 aftershock triggered by the M7.3 earthquake (Table 2). We can find that the coulomb stress changes greatly due to the stress triggering effect. For the M6.6 aftershock, the coulomb stress changes on the focal source decreased 3.1 bar and 4.2 bar based on Gavin

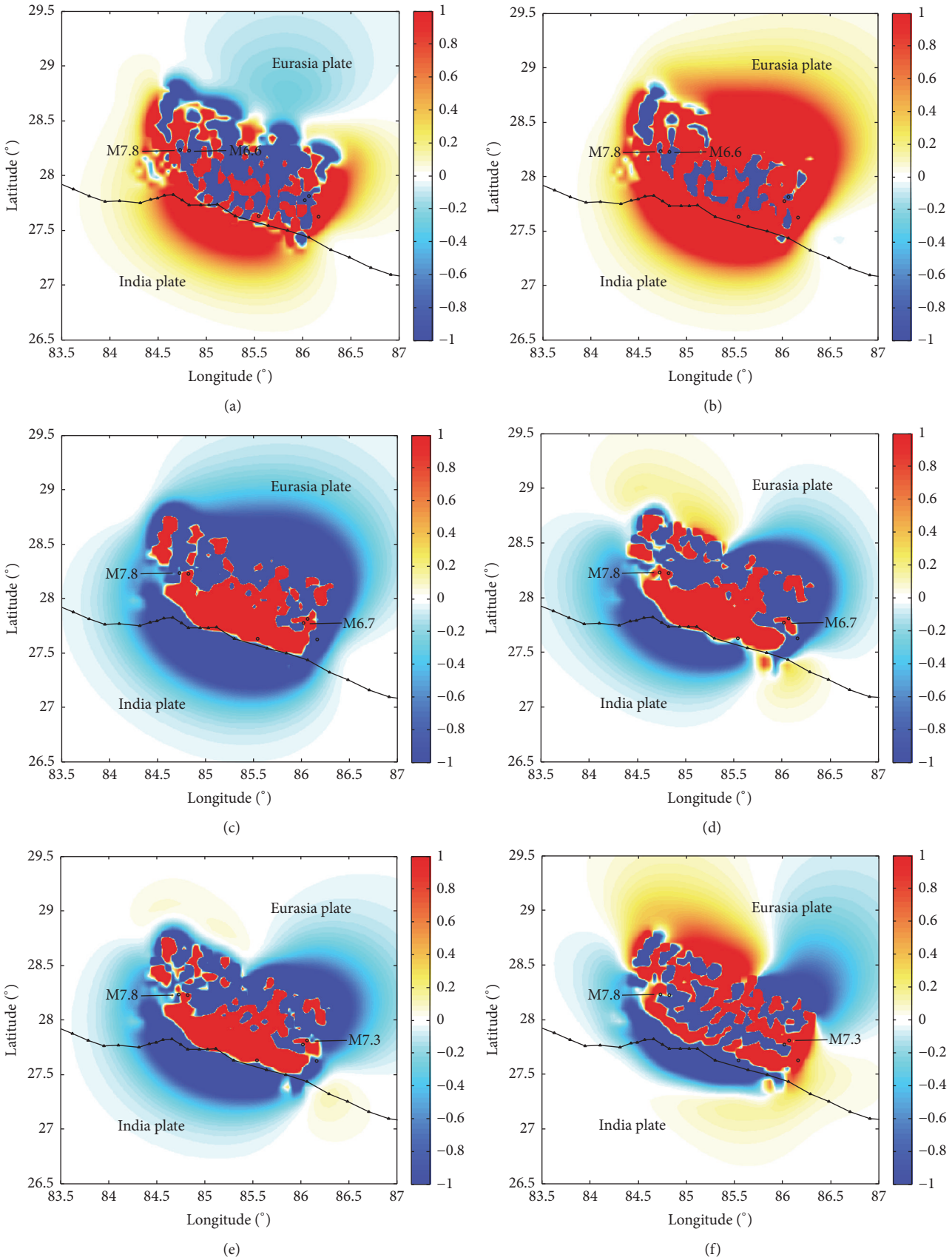

Figure 4: Continued.

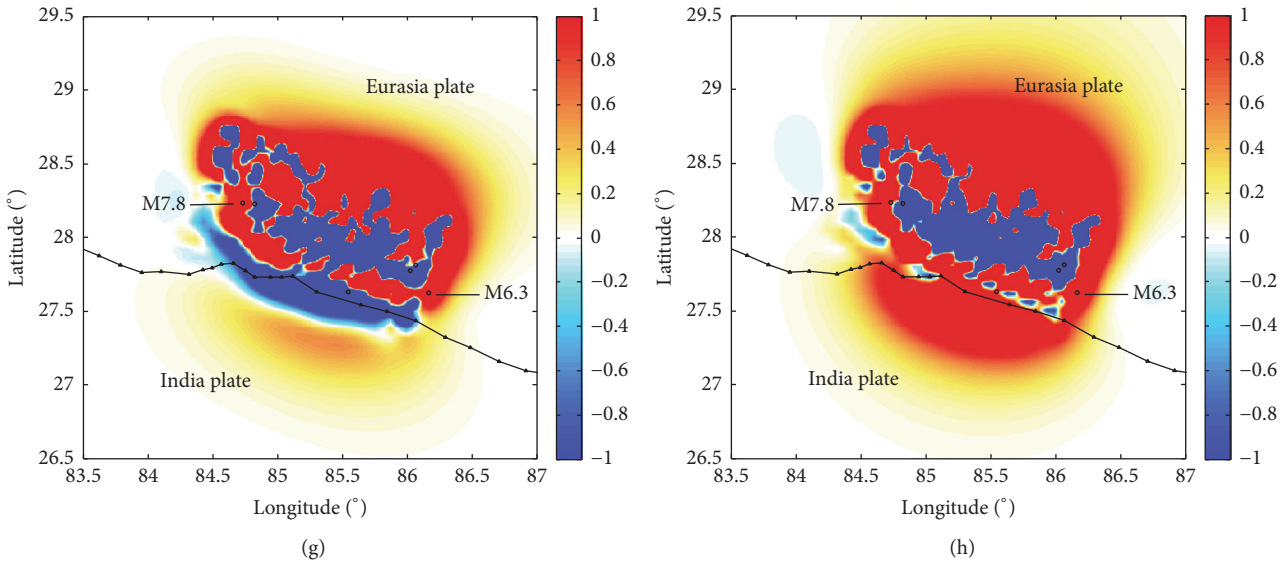

Figure 4: Coulomb stress changes on both nodal planes of 4 M > 6 aftershocks triggered by the 2015 Nepal M7.8 earthquake based on Han Yue's kinematic rupture model (unit: bar). (a) 2015-04-25, M6.6, nodal plane: 271, 21, 64, depth: 10.0 km; (b) 2015-04-25, M6.6, nodal plane: 119, 71, 100, depth: 10.0 km; (c) 2015-04-26, M6.7, nodal plane: 285, 12, 94, depth: 22.9 km; (d) 2015-04-26, M6.7, nodal plane: 100, 78, 89, depth: 22.9 km; (e) 2015-05-12, M7.3, nodal plane: 303, 9, 110, depth: 15.5 km; (f) 2015-05-12, M7.3, nodal plane: 102, 82, 87, depth: 15.5 km; (g) 2015-05-12, M6.3, nodal plane: 274, 14, 89, depth: 15.5 km; (h) 2015-05-12, M6.3, nodal plane: 95, 76, 90, depth: 15.5 km.

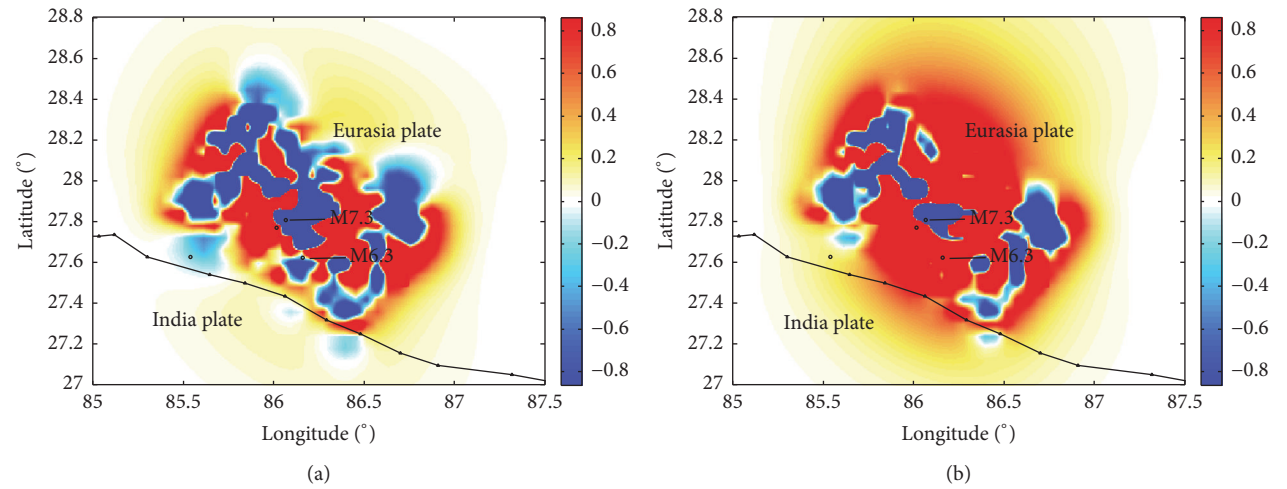

Figure 5: Coulomb stress changes on both nodal planes of M6.3 aftershock triggered by M7.3 earthquake based on Gavin Hayes's finite fault model (unit: bar). (a) Nodal plane: 274, 14, 89, depth: 15.5 km; (b) 95, 76, 90, depth: 15.5 km.

Hayes's model. It decreased 6.1 bar and 4.4 bar, respectively, based on Han Yue's mode, which agrees well with the results in Section 3. For the other three M > 6 aftershocks, the coulomb stress changes on both fault planes increase at varying degrees. The results indicate that most of the aftershocks were triggered by the coulomb stress produced by the M7.8 main shock. In addition, the M7.3 aftershock also promotes or triggers the occurrence of the M6.3 event.

5. Discussion and Conclusions

In this study, the interaction between the Nepal M7.8 main shock and other M > 6 aftershocks was analyzed with the static stress triggering approach. It should be noted that the occurrence of an earthquake is controlled by many factors, among which the geodynamic background is the most important. It is difficult to explain the complex geological phenomenon only by a model or theory. The original intension of this study is to provide a more reliable seismic hazard assessment in the Nepal earthquake zone by considering the interaction of the earthquake sequences.

In this paper, we only analyzed the stress triggering effect of 4 larger aftershocks and did not investigate the other minor aftershocks. The calculation results demonstrate that, depending on two kinds of source models, three in four M > 6 aftershocks received a positive coulomb stress contribution

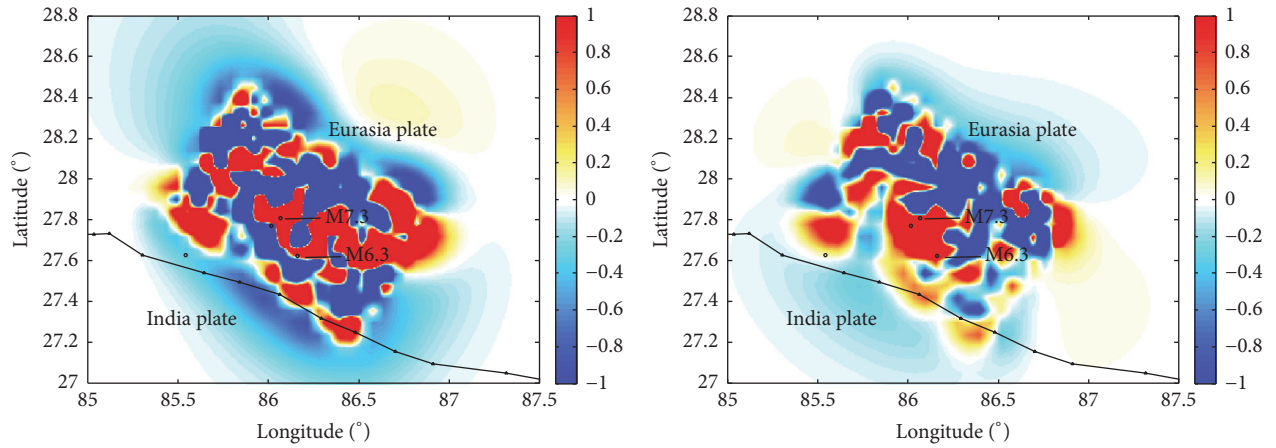

Figure 6: Coulomb stress changes on both nodal planes of M6.3 aftershock triggered by M7.3 earthquake based on Han Yue's kinematic rupture model (unit: bar). (a) Nodal plane: 274, 14, 89, depth: 15.5 km; (b) nodal plane: 95, 76, 90, depth: 15.5 km.

Table 1: The basic parameters of the aftershocks and coulomb stress calculation results.

Aftershock	Coordinates (°)	Depth (km)	Fault plane (°)	Coulomb stress changes based on Hayes's model (bar)	Coulomb stress changes based on Yue's model (bar)
M6.6	28.224	10.0	271,21,64	−3.109	−6.183
	84.822		119,71,100	−4.278	−4.407
M6.7	27.771	22.9	285,12,94	3.259	5.777
	86.017		100,78,89	3.771	6.367
M7.3	27.809	15.5	303,9,110	6.735	2.800
	86.066		102,82,87	1.928	4.688
M6.3	27.625	15.5	274,14,89	0.641	3.440
	86.162		95,76,90	0.620	4.295

from the M7.8 main shock. The stress triggering effect may be magnitude-dependent. Steacy et al. determined that 100% of $M \geqq 5.5$ and 88% of $M \geqq 5$ aftershocks in the first 2 years of the sequence occurred in positive stress lobes of the main shock [24].

As for the stress triggering theory, there are many unquantifiable uncertainties. The uncertain model parameters may affect the calculation results. These parameters include the nodal plane uncertainties, the rigidity, and the stress drop. Data uncertainties are the biggest obstacle to determine quantitatively whether the coulomb stress triggers aftershocks in an earthquake sequence. Our results of post-Nepal M7.8 earthquake stress change is similar to the post-seismic stress change obtained by Lei et al. [25] and Xiong et al. [26] using same values for the coefficient of friction. Both of these studies predict stress evolution in the main frontal thrust interface system close to that of our results.

Based on the seismic stress triggering theory and elastic dislocation theory, firstly, the coulomb stress changes triggered by the Nepal M7.8 earthquake and M7.3 aftershock were calculated. Secondly, the interrelationship among the Nepal earthquake sequence was analyzed and the influence of the M7.8 main shock on the aftershocks distribution was also discussed. Thirdly, the coulomb stress changes on the focal source of each aftershock caused by the M7.8 main shock were further studied. Main conclusions of this study are derived:

(1) The $M > 6$ aftershocks distribution are well explained by the seismic coulomb stress changes caused by the Nepal M7.8 main shock. Three in four $M > 6$ aftershocks occurred in the positive coulomb stress area.

(2) Based on the focal mechanism solutions from USGS, the coulomb stress increment in the focal source of the $M > 6$ aftershocks is about 0.620–6.367 bar except the M6.6 aftershock. The coulomb stress change for the M6.3 aftershock is about 0.1–0.312 bar induced by the M7.3 earthquake. These possible coulomb stress changes are larger than the threshold of stress triggering. Therefore, the occurrence of the $M > 6$ aftershock is probably effectively promoted by the Nepal M7.8 main shock.

Competing Interests

The authors declare that there is no conflict of interests regarding the publication of this paper.

Table 2: The stress changes result of the M6.3 aftershock triggered by the M7.3 earthquake.

Earthquake	Coordinates (°)	Depth (km)	Fault plane (°)	Coulomb stress changes based on Hayes's model (bar)	Coulomb stress changes based on Yue's model (bar)
M6.3	27.625	15.5	274,14,89	0.057	1.215
	86.162		95,76,90	0.100	1.312

Acknowledgments

This work was supported by the Science for Earthquake Resilience (XH15027) and the Earthquake Emergency Youth Key Tasks (CEA_EDEM-201505). The authors wish to thank Professor Gavin Hayes and Dr. Yue Han for the technical support.

References

[1] R. S. Stein, "The role of stress transfer in earthquake occurrence," *Nature*, vol. 402, no. 6762, pp. 605–609, 1999.

[2] S. Steacy, J. Gomberg, and M. Cocco, "Introduction to special section: stress transfer, earthquake triggering, and time-dependent seismic hazard," *Journal of Geophysical Research B: Solid Earth*, vol. 110, no. 5, pp. 1–12, 2005.

[3] Y. Okada, "Internal deformation due to shear and tensile faults in a half-space," *Bulletin of the Seismological Society of America*, vol. 82, no. 2, pp. 1018–1040, 1992.

[4] S. Toda, R. S. Stein, K. Richards-Dinger, and S. B. Bozkurt, "Forecasting the evolution of seismicity in southern California: animations built on earthquake stress transfer," *Journal of Geophysical Research: Solid Earth*, vol. 110, no. 5, pp. 1–17, 2005.

[5] W. Jianchao, L. Dongning, C. Yongjian, and L. Heng, "Stress triggering of the 2012 Sumatra Mw 8.2 earthquake by the 2012 Sumatra Mw 8.6 earthquake," *The Electronic Journal of Geotechnical Engineering*, vol. 20, no. 1, pp. 213–219, 2015.

[6] USGS, "Poster of the April-May 2015 Nepal Earthquakes," 2015, http://earthquake.usgs.gov/earthquakes/eqarchives/poster/2015/NepalSummary.php.

[7] G. Hayes, *Updated Finite Fault Results for the Apr 25, 2015 Mw 7.9 35 km E of Lamjung, Nepal Earthquake (Version 2)*, 2015, http://earthquake.usgs.gov/earthquakes/eventpage/us20002926#finite-fault.

[8] H. Yue, M. Simons, Z. Duputel et al., "Depth varying rupture properties during the 2015 Mw 7.8 Gorkha (Nepal) earthquake," *Tectonophysics*, 2016.

[9] N. E. Dowling, *Mechanical Behavior of Materials: Engineering Methods for Deformation, Fracture, and Fatigue*, Prentice Hall, Upper Saddle River, NJ, USA, 1993.

[10] P. A. Reasenberg and R. W. Simpson, "Response of regional seismicity to the static stress change produced by the Loma Prieta earthquake," *Science*, vol. 255, no. 5052, pp. 1687–1690, 1992.

[11] S. Toda and R. S. Stein, "Response of the San Andreas fault to the 1983 Coalinga-Nuñez earthquakes: an application of interaction-based probabilities for Parkfield," *Journal of Geophysical Research: Solid Earth*, vol. 107, no. 6, pp. ESE 6-1–ESE 6-16, 2002.

[12] R. A. Harris, "Introduction to special section: stress triggers, stress shadows, and implications for seismic hazard," *Journal of Geophysical Research: Solid Earth*, vol. 103, no. 10, pp. 24347–24358, 1998.

[13] M. Cocco and J. R. Rice, "Pore pressure and poroelasticity effects in Coulomb stress analysis of earthquake interactions," *Journal of Geophysical Research: Solid Earth*, vol. 107, no. 2, pp. 1–17, 2002.

[14] D. J. Hart and H. F. Wang, "Laboratory measurements of a complete set of poroelastic moduli for *Berea sandstone* and Indiana limestone," *Journal of Geophysical Research*, vol. 100, no. 9, pp. 17–751, 1995.

[15] T. Parsons, R. S. Stein, R. W. Simpson, and P. A. Reasenberg, "Stress sensitivity of fault seismicity: a comparison between limited-offset oblique and major strike-slip faults," *Journal of Geophysical Research: Solid Earth*, vol. 104, no. 9, pp. 20183–20202, 1999.

[16] D. F. Sumy, E. S. Cochran, K. M. Keranen, M. Wei, and G. A. Abers, "Observations of static Coulomb stress triggering of the November 2011 M5.7 Oklahoma earthquake sequence," *Journal of Geophysical Research: Solid Earth*, vol. 119, no. 3, pp. 1904–1923, 2014.

[17] R. S. Stein and M. Lisowski, "The 1979 Homestead Valley earthquake sequence, California: control of aftershocks and postseismic deformation," *Journal of Geophysical Research: Solid Earth*, vol. 88, no. 8, pp. 6477–6490, 1983.

[18] D. H. Oppenheimer, P. A. Reasenberg, and R. W. Simpson, "Fault plane solutions for the 1984 Morgan Hill, California, earthquake sequence: evidence for the state of stress on the Calaveras fault," *Journal of Geophysical Research*, vol. 93, no. 8, pp. 9007–9026, 1988.

[19] S. Larsen, R. Reilinger, H. Neugebauer, and W. Strange, "Global positioning system measurements of deformations associated with the 1987 Superstition Hills earthquake: evidence for conjugate faulting," *Journal of Geophysical Research*, vol. 97, no. 4, pp. 4885–4902, 1992.

[20] M. D. Zoback and J. Townend, "Implications of hydrostatic pore pressures and high crustal strength for the deformation of intraplate lithosphere," *Tectonophysics*, vol. 336, no. 1–4, pp. 19–30, 2001.

[21] G. Hayes, "Updated Finite Fault Results for the May 12, 2015 Mw 7.3 22 km SE of Zham, China Earthquake (Version 2)," 2015.

[22] C. Ji, D. J. Wald, and D. V. Helmberger, "Source description of the 1999 Hector Mine, California, earthquake, part I: wavelet domain inversion theory and resolution analysis," *Bulletin of the Seismological Society of America*, vol. 92, no. 4, pp. 1192–1207, 2002.

[23] H. Yue, "Kinematic Rupture Process of the 2015 Gorkha (Nepal) earthquake sequence from joint inversion of teleseismic, hr-GPS, strong-ground motion, InSAR interferograms and pixel offsets," in *Proceedings of the GU Fall Meeting*, San Francisco, Calif, USA, December 2015.

[24] S. Steacy, A. Jiménez, and C. Holden, "Stress triggering and the Canterbury earthquake sequence," *Geophysical Journal International*, vol. 196, no. 1, pp. 473–480, 2014.

[25] D. Lei, C. Lian, and Y. Qiao, "The Coulomb Stress Change of Mw 7. 8 Earthquake in Lamjung, Nepal, April 25th, 2015," 2015.

[26] W. Xiong, K. Tan, G. Liu, and Z.-S. Nie, "Coseismic and postseismic Coulomb stress changes on surrounding major faults caused by the 2015 Nepal MW7.9 earthquake," *Chinese Journal of Geophysics-Chinese Edition*, vol. 58, no. 11, pp. 4305–4316, 2015.